Bharanidharan et al., J Theor Comput Sci 2016, 3:2
DOI: 10.4172/2376-130X.1000146

Journal of
Theoretical & Computational Science

Research Article Open Access

Synthesis and Structural Characterization of 2-Hydroxy-5-(Phenyldiazenyl) Benzaldehyde Oxime - A Theoretical Approach

Bharanidharan S[1], Nathiya A[1], Saleem H[1]*, Arokiasamy A[2] and Thanikachalam V[2]

[1]Department of Physics, Annamalai University, Annamalainagar-608 002, Tamil Nadu, India
[2]Department of Chemistry, Annamalai University, Annamalainagar-608 002, Tamil Nadu, India

Abstract

The 2-hydroxy-5-(Phenyldiazenyl)benzaldehyde oxime (PDBO) was synthesized and characterized. The spectral investigations such as FT-IR, FT-Raman and UV-Vis spectra were recorded. The bond parameter values were calculated at DFT/B3LYP/6-311++G(d,p) level of theory. The observed spectral results were compared with the computed wavenumber. The complete vibrational assignments of wavenumbers were made on the basis of TED. The first order hyperpolarizability, intra-molecular charge transfer and band gap energy were studied using B3LYP/6-311++G(d,p) calculation. The electronic transition was studied using UV-Vis spectrum and the observed values were compared with the theoretical values. The MEP, Mulliken charges and thermodynamic parameters of the title molecule was also analyzed using the same level of basis set.

Keywords: FT-IR; FT-Raman; TED; NBO; PDBO

Introduction

The Azo compounds are most versatile molecule and it has received much attention in research in the view of both fundamental and its applications [1,2]. In recent year a large amount of investigation has been carried out for the synthesis and spectroscopic properties of this group of dyes [3-5]. Furthermore, azo compounds are known to be involved in a number of biological reactions such as inhibition of DNA, RNA, and protein synthesis, carcinogenesis, and biological activity against bacteria and fungi [6,7]. The azo dyes produced by aromatic and their oxime derivatives containing at least one azo group (-N=N-) attached to at least one aromatic moiety are the most widely used dyes in textile, printing, leather, paper making, drug and food industries [8]. The azo compounds are very attractive from theoretical and practical viewpoints and have been of particular interest [9-11]. It is described by the intra-molecular charge transfer between the phenol and oxime groups in ground or excited state [12].

Aromatic and heteroaromatic azo compounds constitute the largest and the most diverse group of synthetic dyes with application not only as textile colorants but in many other industrial fields for coloring different substrates, biological-medical studies, in the field of non-linear optics and optical data storage [13-15]. The interest for benzothiazole azo dyes as disperse and cationic dyes for textile application is growing [16]. In recent years, with the development of density functional theory and especially the improvement of time-dependent density functional theory [17], properties of both ground- and excited-states for medium-sized metal complexes can be calculated at the first-principle level with good accuracy [18,19]. To get better insight into the geometry and the electronic structure geometry optimizations of the ground and excited-states were carried out by means of DFT calculations. We also calculate and analyze the three excited states derived from TD-DFT results and compare them with the ground state molecular orbitals (MOs) obtained by DFT calculations.

Computational Details

The entire calculations were performed at DFT/B3LYP/6-311++G(d,p) level of basis set using Gaussian 03W [20] program package, invoking gradient geometry optimization [20,21]. The optimized structural parameters were used in the vibrational frequency calculations at the DFT level to characterize all the stationary points as minima. The vibrationally averaged nuclear positions of PDBO were used for harmonic vibrational frequency calculations resulting in IR and Raman frequencies together with intensities and Raman depolarization ratios. The vibrational modes were assigned on the basis of TED analysis using VEDA4 program [22]. The Raman activity was calculated by using Gaussian 03W package and the activity was transformed into Raman intensity using Raint program [23] by the expression:

$$I_i = 10^{-12} \times (\nu_0 - \nu_i)^4 \times \frac{1}{\nu_i} \times RA_i$$

Where I_i is the Raman intensity, RA_i is the Raman scattering activities, ν_i is the wavenumber of the normal modes and ν_0 denotes the wavenumber of the excitation laser [24].

Experimental Details

Synthesis procedure

A mixture of 5-arylazosalicylaldehyde (1 mmol) and sodium acetate (0.5 g) was dissolved in boiling ethanol and hydroxylamine hydrochloride (0.13 g; 2 mmol) was added. The mixture was refluxed for 3 hr. The reaction mixture was poured into water. The 5-arylazo salicylaldoxime separated out was filtered and recrystallized from ethanol.

Results and Discussion

Molecular geometry

The geometrical parameters such as bond distance (Å), bond angles (°) and torsional angles (°) of PDBO were calculated using B3LYP method with 6-311++G (d,p) basis set. The computed values along with the available experimental data [25] are presented in Table 1 and the

***Corresponding author:** Saleem H, Department of Physics, Annamalai University, Annamalainagar-608 002, Tamil Nadu, India, Tel: +919443879295; E-mail: saleem_h2001@yahoo.com

Received February 21, 2016; **Accepted** May 04, 2016; **Published** May 16, 2016

Citation: Bharanidharan S, Nathiya A, Saleem H, Arokiasamy A, Thanikachalam V (2016) Synthesis and Structural Characterization of 2-Hydroxy-5-(Phenyldiazenyl) Benzaldehyde Oxime - A Theoretical Approach. J Theor Comput Sci 3: 146. doi:10.4172/2376-130X.1000146

optimized structure of PDBO are also shown in Figure 1. The molecule PDBO has two rings namely: i) benzene and ii) phenonilc oxime and the azo chromophore group (-N=N-) is connected in between them. As it is evident from the Table 1, both the Azo benzene rings are coplanar: C2-C3-N12-N13=-180.00 and C4-C3-N12-N13=0.00 and C16-C14-N13-N12=0.00 and C15-C14-N13-N12=-180.00°. The bond angles between C-N and benzene rings are equal: C2-C3-N12=C15-C14-C13=115˚ and C4-C3-N12=C16-C14-N13=124˚ which show there is no steric repulsion in between Azo and benzene rings. In this study, the N=N bond length is 1.253 Å which is supported by literature value 1.25 Å [26,27]. The bond lengths of C3-N12 and C14-N13 are differ by 0.002 Å, which is due to the energy transfer takes place during π(N12=N13) to π*(C2-C3/C14-C15) transitions are differ by $E^{(2)}$ value: 0.01 kj/mol (Table 4). All the calculated C-C and C-H bond distances are in agreement with our earlier work [28] with few exceptions.

Vibrational assignments

The compound PDBO belongs to C_1 point group symmetry and it consists of 29 atoms. Hence 81 normal modes of vibrations are possible and are distributed as: Γ55A′ planar+26″ non-planar). The vibrational wavenumbers and their corresponding assignments are given in Table 2. The vibrational assignments are made on the basis of the total energy distribution (TED) calculations. The theoretical and observed (FT-IR and FT-Raman) spectra are shown in Figures 2 and 3.

The calculated frequencies are slightly higher than the observed values for the majority of the normal modes. Two factors may be responsible for the discrepancies between the experimental and computed spectra of azo compound. The first is caused by the environment and the second reason for these discrepancies is the fact that the experimental value is an enharmonic frequency while the calculated value is a harmonic frequency [29].

O-H vibrations: The OH group vibrations are likely to be most sensitive to the environment, so they show pronounced shifts in the spectra of the hydrogen-bonded species. The non-hydrogen-bonded or a free hydroxyl group absorb strongly in the 3550-3700 cm^{-1} region [30]. In the present study, the calculated/observed OH stretching vibrations are 3685, 3480/3854, 3416 cm^{-1} (mode nos: 1, 2). The phenolic $νO_{23}H_{24}$ vibration observed at higher frequency (~438 cm^{-1}) than the oxime hydroxy ($νO_{29}H_{30}$) mode, which is due to the large ionic character of the phenolic OH group.

The OH in-plane bending vibration in phenol, lies in the region 1270-1150 cm^{-1} [31] and is not much affected due to hydrogen bonding. In our case, the observed FT-IR/FT-Raman bands appeared at 1301/1312 cm^{-1} and its corresponding calculated wavenumber 1311 cm^{-1} (mode no: 23) with TED 14% are belong to βOH mode. The OH out-of-plane deformation vibration in phenol lies in the region 517-710 cm^{-1} for associated OH [32]. In this study, the OH out-of-plane bending vibrations observed at 682 cm^{-1} in FT-IR spectrum and its calculated value is 672 cm^{-1} (mode no: 54). In both inter-molecular and intra-molecular associations, the frequency is at a higher value than in free OH [33]. The frequency increases with hydrogen bond strength because of the larger amount of energy required to twist the O-H bond for out-of plane bending [34]. The mode nos: 26 and 64 are assigned to $βO_{28}H_{29}$ and $ΓO_{28}H_{29}$ modes, respectively.

C-H Vibrations: The hetero aromatic structure shows the presence of C-H stretching vibrations in the region 3200-2900 cm^{-1} [31,35], which is the characteristic region for the ready identification of the C-H stretching vibrations and in this region, the bands are not affected appreciably by the nature of the substituents. In this study, the molecule

Parameters	B3LYP/6-311++G(d,p)	XRD [25]
Bond Lengths (Å)		
C3-N12	1.417	1.428 (9)
N12-N13	1.252	1.257 (9)
N13-C14	1.415	
C16-C19	1.395	1.39
C21-O23	1.367	1.367 (7)
O23-H24	0.962	0.84
C25-H26	1.093	
C25-N27	1.277	1.304 (14)
N27-O28	1.379	
O28-H29	0.974	
Bond Angles (°)		
C2-C3-N12	115.3	
C4-C3-N12	124.7	
C3-N12-N13	115.5	113.4 (7)
N12-N13-C14	115.4	112.2 (7)
N13-C14-C15	115.5	
N13-C14-C16	124.8	
C16-C19-C21	118.5	120
C21-C19-C25	119.2	121.2 (5)
C21-O23-H24	109.9	109.5
Dihedral Angles (°)		
C2-C3-N12-N13	-180.0	
C4-C3-N12-N13	-0.001	
C3-N12-N13-C14	-179.9	
N12-N13-C14-C15	-180.0	
N12-N13-C14-C16	-0.008	
N13-C14-C15-C17	179.9	

Table 1: The selected bond parameters of PDBO.

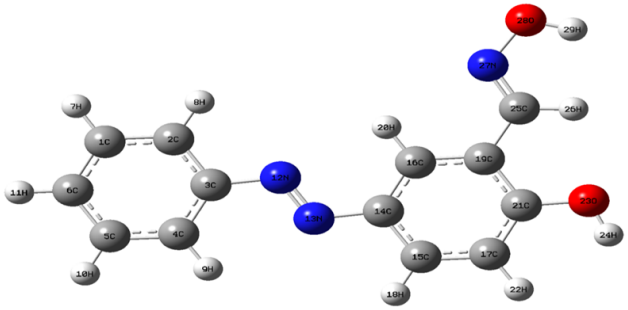

Figure 1: The optimized structure of 2-hydroxy-5-(Phenyldiazenyl) benzaldehyde oxime (PDBO).

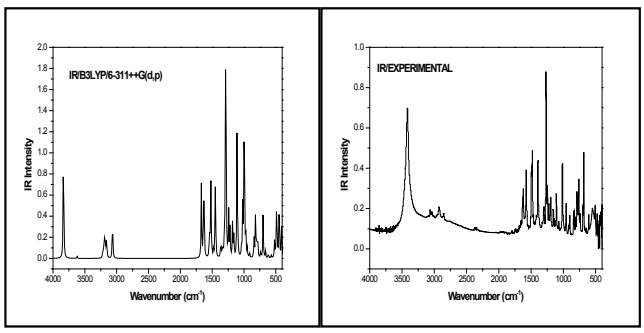

Figure 2: Theoretical and Experimental FT-IR spectra of PDBO.

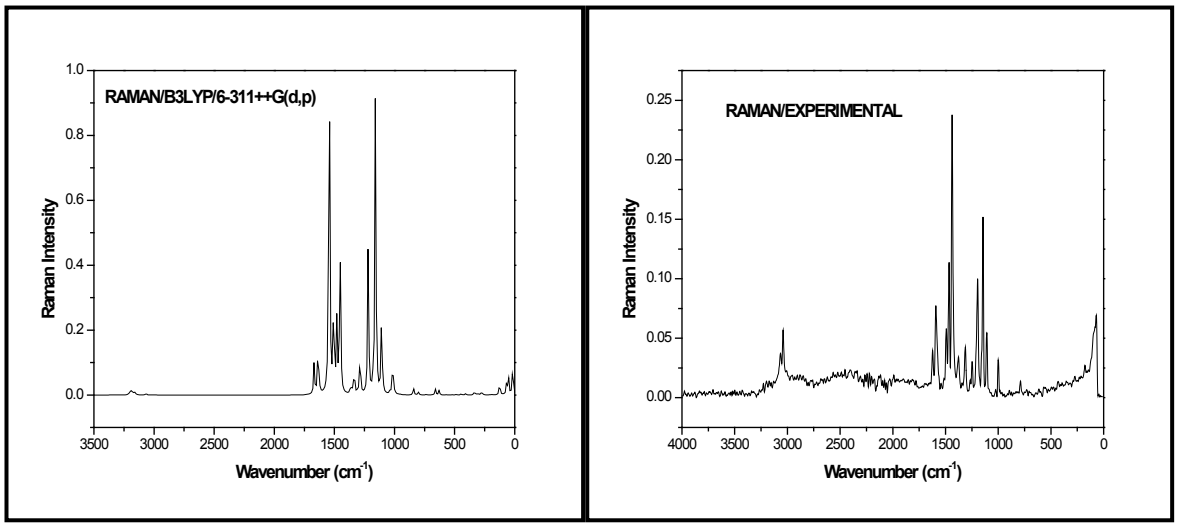

Figure 3: Theoretical and Experimental FT-Raman spectra of PDBO.

PDBO have nine νCH vibrations, which are assigned in the region 3084-2945 cm^{-1} (mode nos: 4 to 11). This assignment is further supported by observed FTIR (3064, 2923 cm^{-1}) and FT-Raman bands (3065, 3040 cm^{-1}) and also find support from literature [33]. Literature survey reveals that the CH in-plane/out-of-plane bending vibrations appear in the ranges 1000-1300 cm^{-1}/750-1000 cm^{-1}, respectively [36,37]. Based on the fact, the harmonic wavenumbers in the regions 1462-1014 cm^{-1} (mode nos: 18-20, 25-27, 31-33, 36)/964-672 cm^{-1} (mode nos: 40, 42-46, 48, 50, 52, 54) are assigned to CH in-plane/out-of-plane bending modes, respectively. These assignments find support from the observed spectral values: βCH (FTIR: 1014, 1142, 1266 cm^{-1})/FT-Raman: 1144, 1437, 1466 cm^{-1}) and ΓCH (FTIR: 899, 832, 789, 759, 682 cm^{-1})/FT-Raman: 789 cm^{-1}) and also in line with literature [28].

C-C vibrations: The benzene ring modes predominantly involve C-C bonds and the vibrational frequency associated with C-C stretching modes of carbon skeleton. In general, the C-C stretching modes, known as semi-circle stretching, modes observed in the range of 1510-1660 cm^{-1} [31]. The phenyl ring C-C stretching vibrations occur in the regions of 1625-1590, 1590, 1575, 1465-1430 and 1380-1280 cm^{-1} were given by Varsanyi [32]. The harmonic wavenumbers in the range 1575-998 cm^{-1} mode nos: 13-16, 19, 21, 23, 24, 28, 30, 36, 37) are assigned to νC-C modes. The observed FTIR: 1575, 1394, 1301, 1248 and 1014 cm^{-1} and FT-Raman: 1591, 1437, 1377, 1312, 1247 and 999 cm^{-1} bands support the νC-C mode. In which the harmonic (1311/mode no: 23)/observed bands 1301: FTIR/1312 cm^{-1}: FT-Raman) are relatively at a higher wavenumber due to its coupling with $\beta O_{23}H_{24}$ bending mode [33]. The coupling C_{19}-C_{25} stretching vibration computed at 1065 cm^{-1} (mode no: 35) show good agreement with recorded FTIR band at 1070 cm^{-1}. In this study, the harmonic C-C-C in-plane and out-of-plane bending modes have been found to be in agreement with the observed spectral values.

(-C-N=N-C-) vibrations: In this study, the Azo chromophoric group can be considered as a single unit, which contains two bonds: C-N and N=N. Each vibrations has its own well known characteristic vibrational frequency. In PDBO the two unequivalent C-N parts C_3-N_{12}: 1.4178 Å and C_{14}-N_{13}: 1.4159 Å causes a change in dipolemoment and hence the N=N stretching is IR active with medium strong intensity (1482 cm^{-1}: FTIR), while the corresponding Raman bands is 1493 cm^{-1} (weak). The N=N stretching vibration of Azo compounds show bands in the region 1380-1450 cm^{-1} [38]. Literature survey reveals, that the bands observed between 1200-1300 cm^{-1} [39,40] belongs to the νC-N modes of Azo compound. The observed FTIR/FT-Raman bands 1107/1108 cm^{-1} and harmonic frequency 1171 cm^{-1} (mode no: 30) and are assigned to νC_3-N_{12} and νC_{14}-N_{13} modes, respectively. These observations indicate that the C-N parts (C_3-N_{12}, C_{14}-N_{13}) of azo group have got increased double bond character [35].

Nonlinear optical properties

NLO materials have been the subject of intense research, due to their possible application in a wide range of technologies, such as optical communication, optical computing and data storage [41-43]. Therefore, it is known that there has been an intense investigation for molecules with large non-zero hyperpolarizabilities, since these substances have potential as the constituents of NLO materials. The azo compound containing systems have a special significance among the many molecular designs that are used for introducing NLO behavior [44,45]. Due to their peculiar photo switching properties, azo benzenes are used in many areas of molecular electronics and suitable for various kinds of applications [46-48].

In this study, the electronic dipole moment, molecular polarizability, anisotropy of polarizability and molecular first hyperpolarizability of PDBO were calculated at B3LYP/6-311++G(d,p) basis set. The mathematical details used for the calculations were reported in our earlier publications [28], and current results are presented in Table 3. It is well-known that the higher values of dipole moment, molecular polarizability, and hyperpolarizability which enhances the NLO property.

Urea is one of the prototypical molecule used in the study of the NLO property of molecular systems, and thus, it was used frequently as a threshold value for comparative purposes. The first hyperpolarizability value of PDBO was calculated as 16.93289×10^{-30} esu using B3LYP/6-311++G(d,p) method. According to these result, the β_0 value of present molecule is 45 times larger than the magnitude of urea.

NBO analysis

The NBO analysis was performed on PDBO using B3LYP method with 6-311++G(d,p) basis set and the results are listed in the Table

4. NBO analysis provides an efficient method for studying intra- and inter-molecular bonding and interaction among bonds, and also provides a convenient basis for investigating charge transfer or conjugative interaction in molecular systems. Some electron donor orbital, acceptor orbital and the interacting stabilization energy resulted from the second-order micro-disturbance theory are reported [49,50]. The larger $E^{(2)}$ value the more intensive is the interaction between electron donors and acceptor i.e., the more donation tendency from electron donors to electron acceptors and the greater the extent of conjugation of the whole system [51]. Delocalization of electron density between occupied Lewis - type (bond or lone pair) NBOs and formally unoccupied (anti bond or Rydeberg) non Lewis NBOs correspond to a stabilizing donor-acceptor interaction.

The lower electron density of donor and higher electron density of acceptor have maximum delocalization, which results strong bond interaction. In general, the bonds having higher electron density value with lower $E^{(2)}$ energy which causes the vibrational frequency shifts. The electron density $E^{(2)}$ energy value for C_3-N_{12} and C_{14}-N_{13} are 1. 9794 e/4.18 kj/mol and 1.9793 e/7.15 kj/mol, respectively and their corresponding harmonic values are 1113 and 1171 cm^{-1} mode nos: 34 and 30), which are negatively deviated from literature (1200-1300 cm^{-1}) [39,40]. The LP O_{23}-π transfer more energy to acceptor bond π* C_{17}-C_{21} (116.11 kj/mol), while the LPO_{23}-π transfer lesser energy to C_{25}-N_{27} bond (84.52 kj/mol). This may be one of the reason for the phenolic O_{23}-H_{24} stretching observed at higher frequency 3854 cm^{-1} than the oxime hydroxy OH νO_{28}-H_{29}: 3416 cm^{-1}.

In this study the bonds σN_{12}-N_{13} and πN_{12}-N_{13} having the electron density 1.9868 e and 1.9143 e, which stabilizes 7.11 and 42.43 kj/mol, respectively to its antibonding orbitals of σ*(C_2-C_3) and π*(C_2-C_3). The more energy transfer takes place during π to π* transition rather than σ to σ*. The maximum stabilization energy $E^{(2)}$ associated with resonance interaction π(C_{16}-C_{19})→π*(C_{17}-C_{21}) is obtained as 103.22 kj/mol, which is due to the O_{23}-H_{24} group attached with C21 atom.

UV-Visible analysis

The UV-Vis absorption spectra of PDBO molecule were calculated using TD-DFT method with B3LYP/6-311++G(d,p) basis set. The observed and calculated UV-Visible spectra are shown in Figure 4 and their values are presented in Table 5.

The absolute errors between the theoretical and experimental emission λ_{max} values decreases evidently when solvent effects are considered with the TD-DFT method. When the title compound is excited at 329, 363 and 478 nm in calculated spectrum, on the other hand the experimental spectrum observed at 280, 350 and 430 nm in three excited states. The calculated results are in excellent agreement with the experimental values. In addition, there is only one main absorption, as well as one emission wavelengths with the strongest oscillator strength. These wavelengths correspond to the π-π* excitation of the solely highest occupied (HOMO) to lowest unoccupied (LUMO) molecular orbital with the largest transitional proportion.

Homo and Lumo analysis

The Homo of the title molecule is localized on the unity of the azo and the Lumo is located on the oxime region as shown in Figure 5. However, Homo-2 and Lumo+1 are localized mainly on the benzene ring of the azo and oxime groups, respectively. Thus, the transition from Homo to Lumo is easier than that from Homo-1 to Lumo, Homo to Lumo+1, Homo-1 to Lumo+1 and Homo-2 to Lumo+2. This phenomenon also elucidates why the lowest energy absorption is a charge transfer transition from Homo to Lumo and mainly an electronic transition. Therefore, the electron density decreases significantly in the electron-donating azo when electrons transfer from the Homo to Lumo. This phenomenon is accompanied by an increase in the electron density of the electron-accepting the moiety. This result indicates that the electrons transfer from the unit of the azo to oxime group. The Homo and Lumo energies for PDBO calculated at -6.269502 eV and -2.509433 eV, respectively, where as the Homo-Lumo energy gap is 3.760069 eV.

In addition to this, the various quantum chemical parameters such as: Ionization potential, electron affinity, electrophilicity index, chemical potential, electro negativity and hardness are calculated using the standard procedure [28] and are listed in Table 6.

MEP analysis

The MEP surface map was calculated at B3LYP/6-311++G(d,p) method. MEP is related to the electronic density. It is very useful descriptor in understanding sites for electrophilic attacks and nuleophilic reactions as well as hydrogen bonding interactions [52]. The importance of MEP lies in the fact that it simultaneously displays molecular size, shape as well as positive, negative and neutral electrostatic potential regions in terms of colour grading as shown in Figure 6.

Potential increases in the order red<orange<yellow<green<blue. The colour code of these maps is in the range between -7.271 e-2

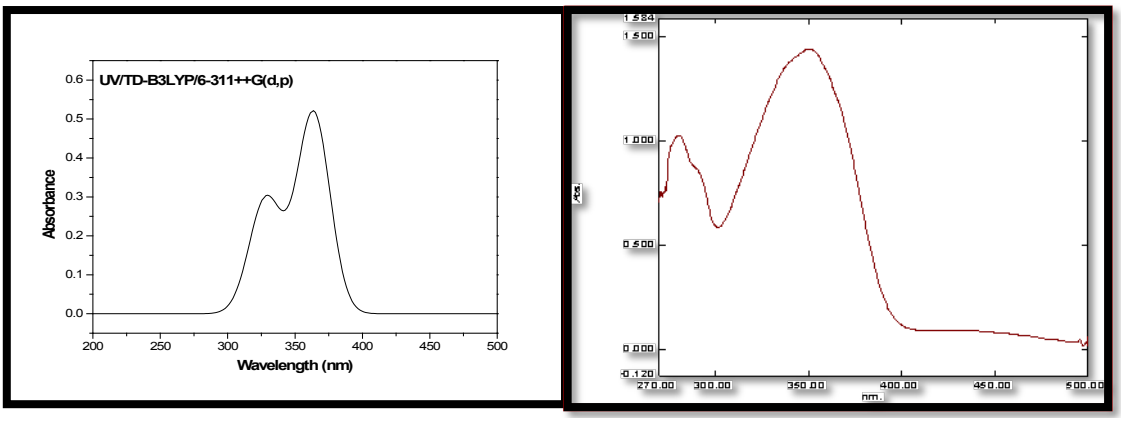

Figure 4: Theoretical and Experimental UV-Visible spectra of PDBO.

Mode No	Calculated Frequencies (cm^{-1})	Observed Frequencies (cm^{-1})		IR Intensity	Raman Intensity	Reduced Masses	Force Consts	Vibrational Assignments ≥ 10% (TED)[d]
	Scaled[a]	FT-IR	FT-Raman	Rel.[b]	Rel.[c]			
1	3685	3854		45.53	0.62	1.07	9.24	VO23H24(100)
2	3480	3416		0.79	0.91	1.07	8.24	VO28H29(100)
3	3095			1.39	0.04	1.09	6.66	VC16H20(99)
4	3084			1.63	0.24	1.09	6.63	VC4H9(92)
5	3070			0.14	0.76	1.09	6.58	VC1H7(92)
6	3070			5.64	0.44	1.10	6.59	VC15H18(82)
7	3061	3064	3065	6.64	0.89	1.09	6.53	VC1H7(85)
8	3050			3.67	0.62	1.09	6.47	VC2H8(88)
9	3040		3040	0.84	0.19	1.09	6.40	VC1H7(84)
10	3033			6.95	0.71	1.09	6.40	VC17H22(45)+VC25H26(41)
11	2945	2923		15.63	0.47	1.09	6.02	VC17H22(99)
12	1603	1622	1622	26.05	8.48	7.68	12.61	VN27C25(76)
13	1575	1575	1591	2.42	6.19	6.38	10.10	VN12N13(10)+VC1C2(47)
14	1569			15.46	5.81	6.42	10.08	VC1C2(48)+VC19C25(13)
15	1562			9.07	0.70	6.52	10.16	VC2C3(39)+βC14C16C19(11)
16	1557			5.58	0.47	5.87	9.08	VC1C2(36)+VC1C2(10)+βC1C2C3(12)
17	1483	1482	1493	9.08	100.00	6.52	9.15	VN12N13(63)
18	1462		1466	26.94	0.17	2.87	3.92	βH20C16C19(45)
19	1447		1437	3.61	25.25	2.34	3.13	VC1C2(12)+βH8C2C1(38)
20	1421			2.20	18.55	2.38	3.07	βH7C1C6(48)
21	1396	1394	1377	17.04	41.49	4.24	5.27	VC1C2(48)
22	1390			14.42	1.74	1.52	1.87	βH29O28N27(47)+βH26C25N27(23)
23	1311	1301	1312	5.38	2.27	4.08	4.48	VC14C16(66)+βH24O23C21(14)
24	1296			0.92	0.55	4.04	4.32	VC1C2(64)+ βH7C1C6(13)
25	1283			2.56	5.94	1.42	1.49	βH29O28N27(12)+βH7C1C6(49)+βH26C 25N27(10)
26	1282			1.06	0.71	1.42	1.49	βH29O28N27(22)+βH8C2C1(36)
27	1254	1266		7.38	0.83	1.74	1.75	VN12C3(11)+βH18C15C17(49)
28	1236	1248	1247	100.00	10.65	4.52	4.41	VC15C17(62)
29	1192	1195	1195	15.18	0.09	2.23	2.02	VN12C3(18)
30	1171			9.69	38.71	2.09	1.83	VC16C19(14)+VN13C14(12)+βH24O23 C21(15)
31	1135	1142	1144	0.61	0.84	1.15	0.94	βH7C1C6(61)
32	1133			8.71	0.13	1.27	1.04	βH24O23C21(23)+βH18C15C17(39)
33	1131			3.00	1.16	1.37	1.12	βH9C4C5(40)
34	1113	1107	1108	7.42	83.07	2.26	1.79	VN12C3(27)+βH9C4C5(10)
35	1065	1070		45.21	18.06	1.92	1.39	VC19C25(17)+βH18C15C17(23)
36	1054	1014		3.89	2.28	1.51	1.07	VC5C6(31)+βH7C1C6(11)+βH7C1C6(24)
37	998		999	3.29	0.59	2.05	1.30	VC1C6(46)+βH10C5C6(24)+βC4C5C6(14)
38	979			16.80	0.41	2.82	1.72	βH20C16C19(10)+βC3N12N13(10)+βC14 C16C19(10)

39	975			0.29	9.18	6.15	3.73	VC1C6(25)+βC1C6C5(20)+βC2C1C6(43)
40	964			0.03	0.04	1.29	0.77	τH7C1C6C5(62)+τH2C1C6C5(19)
41	957	956		64.86	0.66	8.20	4.79	VO28N29(67)
42	953			0.00	0.00	1.36	0.79	τH9C4C5C6(82)
43	934			6.87	0.10	1.48	0.82	τH20C16C19C21(77)
44	913			1.56	0.12	1.37	0.73	τH18C15C17C21(80)
45	910			1.66	0.02	1.45	0.77	τH11C6C5C4(79)
46	905	899		0.01	0.03	1.39	0.72	τH20C16C19C21(72)
47	876			1.50	0.06	6.33	3.10	βC14C15C17(24)+βC2C1C6(13)
48	820	832		0.02	0.00	1.25	0.54	τH7C1C6C5(96)
49	809			7.12	1.82	5.76	2.41	VC15C17(33)+βC15C14C16(18)
50	785	789	789	16.88	0.02	1.51	0.60	τH18C15C17C21(69)
51	770			3.82	0.78	6.22	2.36	VN12C3(13)+βC1C6C5(21)+βC14C15C17(11)
52	754	759		9.07	0.08	1.78	0.65	τH9C4C5C6(32)+τH7C1C6C5(16)+ΓN12C2C4C3(18)
53	709			2.30	0.15	4.15	1.33	τC3C2C1C6(12)+ΓC25C16C21C19(50)
54	672	682		14.26	0.00	1.90	0.55	τH9C4C5C6(50)+τC2C1C6C5(15)+ΓC17C21O23H24(25)
55	635			2.47	0.82	6.15	1.58	βC14C16C19(18)+βC14C15C17(16)+βC25N27O28(33)
56	633			0.10	0.80	6.98	1.78	βC3N12N13(42)
57	604	606	613	0.07	1.18	6.53	1.52	βC2C1C6(72)
58	592		598	1.66	0.01	3.62	0.81	τC2C1C6C5(11)+τC3C2C1C6(34)+τC14N13N12C3(11)
59	549	550		0.97	0.09	4.65	0.89	βC3N12N13(58)+ΓC19C21O23H24(20)
60	501	506		3.55	0.00	3.32	0.53	τC2C1C6C5(14)+τC3C2C1C6(11)+ΓN12C2C4C5(31)
61	496			3.70	0.07	7.24	1.14	VN15C17(14)+βC15C14C16(18)
62	469	476		16.13	0.16	7.38	1.04	βC14N13N12(15)+βC14C16C19(34)
63	459	454		5.39	0.00	3.13	0.42	τC19C25N27O28(68)
64	429	423	432	22.46	0.33	1.28	0.15	τH29O28N27C25(91)
65	403			0.00	0.00	2.96	0.31	τC1C6C5C4(78)
66	392			0.02	0.26	5.35	0.53	τC3C2C1C6(10)+τC14C15C17C21(54)
67	391			13.52	0.09	5.73	0.56	βC3N12N13(11)+βC3N12N13(57)
68	322			2.50	0.92	6.95	0.46	βC14C16C19(25)
69	305			19.44	0.18	1.85	0.11	τH24O23C21C17(57)+τH24O23C21C17(15)
70	293			14.61	0.33	1.68	0.09	τH3C2C1C6(12)+τH24O23C21C17(59)
71	267		273	0.29	0.53	5.69	0.26	VN13C14(11)+βC15C14C16(10)+βC14N13N12(35)
72	257			0.00	0.40	5.79	0.24	τC16C14C15C17(50)
73	200			1.22	0.05	6.55	0.17	VN13C14(11)+βC3C12C13(44)
74	182		177	0.01	0.09	8.17	0.17	τC2C3N12N13(22)+τC15C17C21C19(36)
75	122			9.09	1.79	3.46	0.03	ΓC16C15N13C14(68)
76	119			1.57	1.33	6.66	0.06	βC3N12N13(75)
77	91			3.64	0.08	5.11	0.03	τC21C19C25N27(12)+τC2C3N12N13(46)+τC2C1C6C5(11)

78	66		70	5.55	2.58	3.64	0.01	τC2C1C6N5(79)
79	51			0.59	5.36	6.56	0.01	βC14N13N12(79)
80	47			2.01	0.02	6.09	0.01	τC14N13N12C3(39)+τC14C15C17C21(19) +ΓN12C2C4C3(14)
81	16			0.09	8.09	4.05	0.00	τC2C3N12N13(87)

[a]Scaling factor: 0.9608 ,[b]Relative IR absorption intensities normalized with highest peak absorption equal to 100,[c]Relative Raman intensities calculated by Equation (1) and normalized to 100. [d]TED calculated at B3LYP/6-311++G(d,p) level.

Table 2: The vibrational assignments of PDBO.

Parameters	B3LYP/6-311++G(d,p)
Dipole moment (μ) Debye	
μ_x	-0.708
μ_y	-1.580
μ_z	-0.0001
μ	1.731**Debye**
Hyperpolarizability (β_0) × 10^{-30} esu	
β_{xxx}	1864.227
β_{xxy}	180.539
β_{xyy}	-19.196
β_{yyy}	-322.478
β_{xxz}	0.170
β_{xyz}	0.036
β_{yyz}	0.019
β_{xzz}	106.305
β_{yzz}	-41.978
β_{zzz}	0.003
β_0	16.932 **× 10^{-30} esu**

Table 3: The NLO measurements of PDBO.

Type	Donor NBO (i)	ED/e	Acceptor NBO (j)	ED/e	$E^{(2)}$ kj/mol	E(j)-E(i) a.u.	F(i,j) a.u.
σ -σ*	BD (1) C2 - C3	1.9753	BD*(1) C1 - C2	0.01416	10.6	1.28	0.051
			BD*(1) C1 - H7	0.01379	9.7	1.14	0.046
			BD*(1) C3 - C4	0.03365	15.8	1.26	0.062
			BD*(1) C4 - H9	0.01564	9.0	1.15	0.045
			BD*(1) N12 - N13	0.00763	8.4	1.28	0.045
π -π*	BD (2) C2 - C3	1.6128	BD*(2) C1 - C6	0.32408	80.4	0.28	0.067
			BD*(2) C4 - C5	0.28956	80.8	0.28	0.068
			BD*(2) N12 - N13	0.21273	86.1	0.23	0.064
σ -σ*	BD (1) C3 - N12	1.9794	BD*(1) C1 - C2	0.01416	7.4	1.35	0.044
			BD*(1) C2 - C3	0.02184	4.1	1.33	0.033
			BD*(1) C3 - C4	0.03365	6.1	1.33	0.039
			BD*(1) C4 - C5	0.01452	4.8	1.36	0.035
			BD*(1) N13 - C14	0.03018	19	1.18	0.066
σ -σ*	BD (1) N12 - N13	1.9868	BD*(1) C2 - C3	0.02184	7.1	1.54	0.046
			BD*(1) C14 - C15	0.02186	7.4	1.52	0.046
π -π*	BD (2) N12 - N13	1.9143	BD*(2) C2 - C3	0.36971	42.4	0.4	0.061
			BD*(2) C14 - C15	0.39365	42.1	0.39	0.061
σ -σ*	BD (1) N13 - C14	1.9793	BD*(1) C3 - N12	0.03041	18.8	1.19	0.065
			BD*(1) C14 - C15	0.02186	4.4	1.33	0.034
			BD*(1) C14 - C16	0.03187	7.1	1.34	0.043
			BD*(1) C15 - C17	0.01286	7.2	1.34	0.043
			BD*(1) C16 - C19	0.0192	5.0	1.34	0.036
π -π*	BD (2) C16 - C19	1.6515	BD*(2) C14 - C15	0.39365	72.2	0.28	0.063
			BD*(2) C17 - C21	0.38858	103.2	0.27	0.073
			BD*(2) C25 - N27	0.16239	67.9	0.27	0.062
σ -σ*	BD (1) C17 - C21	1.978	BD*(1) C15 - C17	0.01286	12.8	1.3	0.057
			BD*(1) C15 - H18	0.01333	9.58	1.17	0.046
			BD*(1) C19 - C21	0.03049	18.2	1.26	0.066
			BD*(1) C19 - C25	0.02776	12.0	1.19	0.052

π -π*	BD (2) C17 - C21	1.6503	BD*(2) C14 - C15	0.39365	96.3	0.3	0.075
			BD*(2) C16 - C19	0.33865	61.9	0.3	0.06
σ -σ*	BD (1) O23 - H24	1.9878	BD*(1) C19 - C21	0.03049	17.2	1.3	0.065
σ -σ*	BD (1) C25 - H26	1.981	BD*(1) C16 - C19	0.0192	16.2	1.13	0.059
			BD*(1) N27 - O28	0.02116	6.4	0.79	0.031
σ -σ*	BD (1) C25 - N27	1.9917	BD*(1) C19 - C21	0.03049	5.4	1.45	0.039
			BD*(1) C19 - C25	0.02776	8.5	1.38	0.048
π -π*	BD (2) C25 - N27	1.9519	BD*(2) C16 - C19	0.33865	31.3	0.37	0.051
σ -σ*	BD (1) N27 - O28	1.9886	BD*(1) C19 - C25	0.02776	12.8	1.32	0.057
σ -σ*	BD (1) O28 - H29	1.9937	BD*(1) N27 - O28	0.02116	5.4	0.99	0.032
n -σ*	LP (1) O23	1.978	BD*(1) C17 - C21	0.02449	23.9	1.17	0.073
n -π*	LP (2) O23	1.872	BD*(2) C17 - C21	0.38858	116.1	0.36	0.095

Table 4: The NBO analysis for PDBO.

Calculated at B3LYP/ 6-311++G(d,p)	Oscillator strength	Calculated Band gap (ev/nm)	Experimental Band gap (nm)	Assignments
Excited State 1	Singlet-A (f=0.0000)	2.5897 eV/478.75 nm	430	π-π*
62 -> 64	0.66567	3.953529		
Excited State 2	Singlet-A (f=0.5172)	3.4096 eV/363.64 nm	350	π-π*
61 -> 64	0.17914	4.328773		
63 -> 64	0.60836	3.760057		
63 -> 65	0.18689	4.506191		
Excited State 3	Singlet-A (f=0.2955)	3.7765 eV/328.30 nm	280	π-π*
61 -> 64	0.60751	4.328773		
63 -> 64	-0.18306	-3.760057		
63 -> 65	0.18127	4.506191		

Table 5: The electronic transitions of PDBO.

Parameters	Values
HOMO	-6.269 eV
LUMO	-2.509 eV
Energy gap	-3.760 eV
Ionization potential (IP)	-6.269 eV
Electron affinity (EA)	-2.509 eV
Electrophilicity Index (ω)	2.562
Chemical Potential (μ)	4.389
Electro negativity (χ)	-4.389 eV
Hardness (η)	-3.760

Table 6: The Physico-Chemical properties of PDBO.

(red) and 7.271 e-2 (blue) in the compound, where blue indicates the strongest interaction and red indicates the strongest repulsion. The regions of negative V(r) are usually associated with the lone pair of electronegative atoms, (oxygen and nitrogen); the regions having the positive potential are over the hydrogen atoms. From these results, we can say that the hydrogen atoms indicate the strongest attraction and oxygen, nitrogen atoms indicates the strongest repulsion.

Mulliken atomic charges

The mulliken atomic charges plot of the title molecule is shown in Figure 7. The charges was calculated at B3LYP/6-311++G(d,p) level of basis set and are listed in Table 7. It reveals that when compared to N_{12}, N_{13} is considered as more basic site, which also support to the proton migration from hydroxyl group. The charge distribution shows that the more negative charge is concentrated on oxygen atom where as the partial positive charge resides at hydrogen. In PDBO the C19/C21 atoms have got most positive/negative charges, which are due to the attachment of oxime O23-H24 groups, respectively.

Temperature dependence of thermodynamic properties

Figure 8 depicts the correlation of heat capacity at constant pressure (Cp), enthalpy change $(H^0\text{-}E^0)/T$, Gibb's free energy $(G^0\text{-}E^0)/T$, entropy (S), and (E) thermal energy with temperature by B3LYP/6-311++G(d,p) method.

It cal be observed from the Table 8, that thermodynamic functions are increasing with temperature ranging (100 to 1000°K). This may be due to the fact that the different energy values in accordance with equipartition theorem corresponding to the 3N degrees of freedom may increase with increases in temperature, which in turn increase the internal energy of the molecules and thus the other thermodynamic parameters. The correlation equations between heat capacity, entropy, enthalpy changes and temperatures were fitted by quadratic fomula. The corresponding fitting factors (R^2) 0.99952, 0.99999 and 0.99946, respectively and their corresponding fitting equations are as follows:

$C^0_{p,m}=4.45407+0.0186T+1.64807 \times 10^{-5}\ T^2$ ($R^2=0.99952$)

$S^0_m=1.08583+0.00453T-4.01775 \times 10^{-5}\ T^2$ ($R^2=0.99999$)

$\Delta H^0_m=3.73263+0.01559T+1.38113 \times 10^{-5}\ T^2$ ($R^2=0.99946$)

Conclusion

The title molecule was synthesized and characterized by spectral analysis such as FT-IR, FT-Raman and UV-Visible studies. A complete vibrational analysis has been performed for the first time for PDBO molecule. The bond parameters were calculated and compared with the related XRD data. The bond angles between C-N and benzene rings are

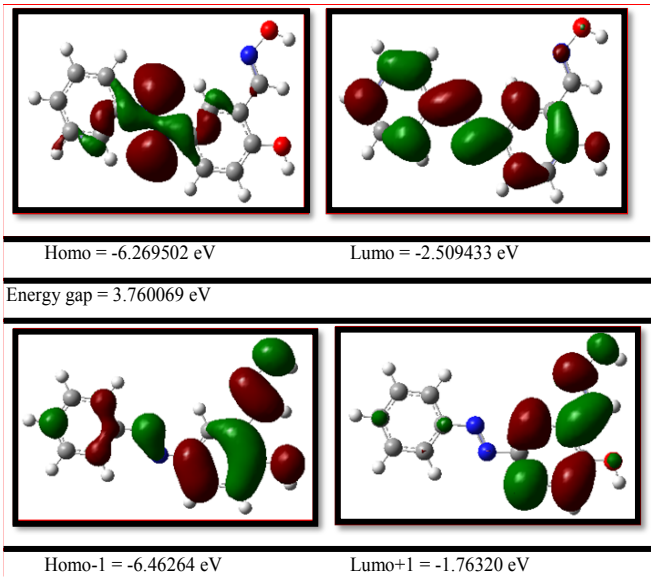

Figure 5: The frontier molecular orbitals for PDBO.

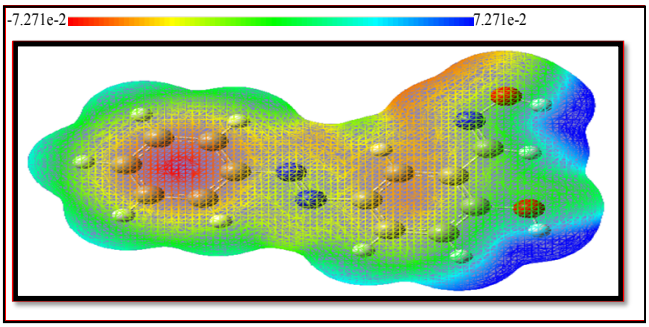

Figure 6: Molecular electrostatic potential map of PDBO.

Atoms	Charges	Atoms	Charges
1C	-0.130	16C	-0.405203
2C	-0.068	17C	0.051539
3C	-0.391	18H	0.177496
4C	0.155	19C	1.752138
5C	-0.182	20H	0.29974
6C	-0.358	21C	-2.218842
7H	0.186	22H	0.154298
8H	0.159	23O	-0.211696
9H	0.185	24H	0.265845
10H	0.185	25C	0.546891
11H	0.148	26H	0.163336
12N	0.089	27N	-0.375776
13N	0.096	28O	0.128423
14C	-0.924	29H	0.227259
15C	0.293		

Table 7: The Mulliken charges of PDBO.

T (K)	S (J/mol.K)	Cp (J/mol.K)	ddH (kj/mol)
100	357.4	109.3	7.2
200	455.4	182.8	21.8
300	544.1	259.5	43.9
400	628.7	330.6	73.5
500	709.1	389.9	109.6
600	784.6	437.3	151.1
700	855	475.1	196.8
800	920.5	505.6	245.9
900	981.5	530.7	297.7
1000	1038.5	551.6	351.9

Table 8: Thermodynamic properties at different temperatures of PDBO.

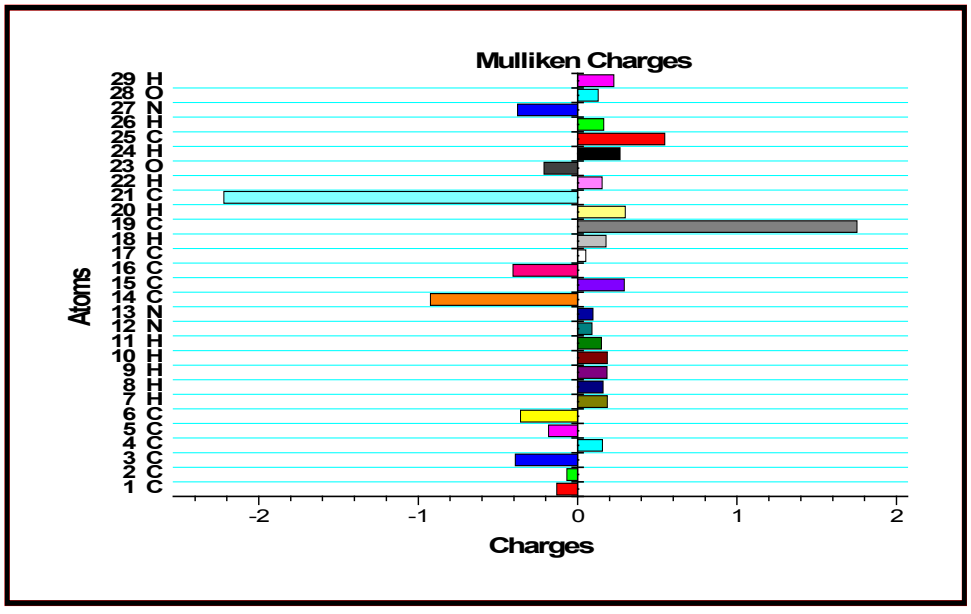

Figure 7: The Mulliken atomic charges of PDBO.

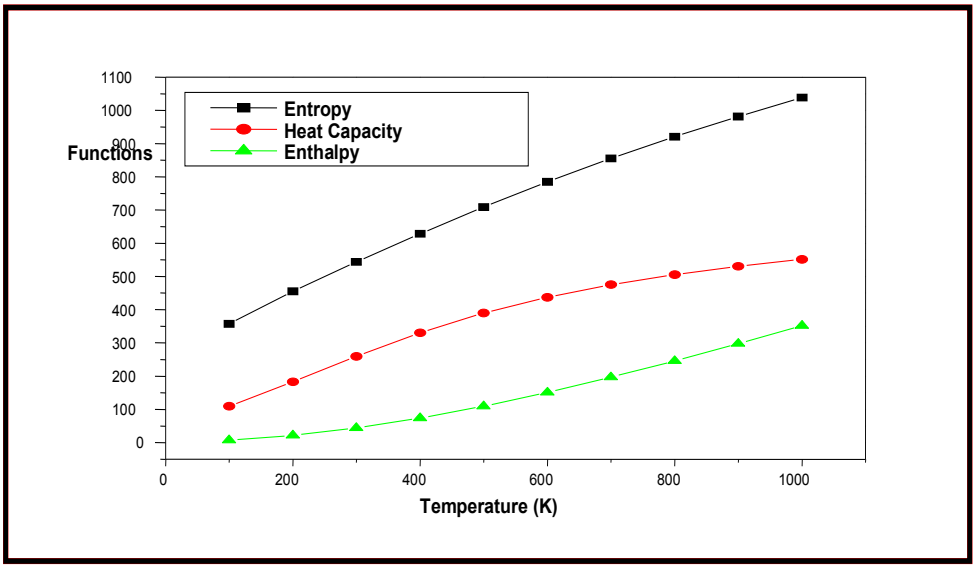

Figure 8: Thermodynamics and different temperatures of PDBO.

equal: C_2-C_3-N_{12}=C_{15}-C_{14}-C_{13}=115° and C_4-C_3-N_{12}=C_{16}-C_{14}-N_{13}=124° which show there is no steric repulsion in between the Azo rings of PDBO. The -C-N=N-C- vibration indicate that the two unequivalent C-N parts (C_3-N_2, C_{14}-N_{13}), which causes a change in dipole moment and hence the azo group has increased double bond character. The β_0 value of PDBO is forty five times larger than magnitude of urea; hence the molecule has good NLO property. The νO_{23}-H_{24} mode observed at higher frequencies due to the high energy transfer from LPO_{23} to π^*C_{17}-C_{21} anti-bonding orbital. UV-Visible absorption analysis the Experimental band at 350 nm is attributed mainly due to a HOMO → LUMO transition is predicted as π-π* transition. The physico-chemical properties and mulliken atomic charges were calculated. The thermodynamic functions have been plotted at different temperatures of PDBO molecule.

References

1. Nejati K, Rezvani Z, Massoumi B (2007) Syntheses and investigation of thermal properties of copper complexes with azo-containing Schiff-base dyes. Dyes Pigm 75: 653-657.
2. Peker E, Serin S (2004) Synth React Inorg Met. Org Chem 34: 859-864.
3. Karci F, Ertan N (2005) Synthesis of some novel hetarylazo disperse dyes derived from 4-hydroxy-2H-1-benzopyran-2-one (4-hydroxycoumarin) as coupling component and investigation of their absorption spectra. Dyes Pigm 64: 243-249.
4. Karci F, Sener NI, Deligöz H (2003) Azocalixarenes. 1: synthesis, characterization and investigation of the absorption spectra of substituted azocalix[4]arenes. Dyes Pigm 59: 53-61.
5. Karci F, Sener NI, Deligöz H (2004) Azocalixarenes. 2: synthesis, characterization and investigation of the absorption spectra of azocalix[6] arenes containing chromogenic groups. Dyes Pigm. 62: 131-140.
6. Vicente S, Maniasso N, Queiroz ZF, Zagatto EA (2002) Spectrophotometric flow-injection determination of nickel in biological materials. Talanta 57: 475-480.
7. Khedr AM, Gaber M, Issa RM, Erten H (2005) Synthesis and spectral studies of 5-[3-(1,2,4-triazolyl-azo]-2,4-dihydroxybenzaldehyde (TA) and its Schiff bases with 1,3-diaminopropane (TAAP) and 1,6-diaminohexane (TAAH). Their analytical application for spectrophotometric microdetermination of cobalt(II). Application in some radiochemical studies. Dyes Pigm 67: 117-126.
8. Torres E, Bustos-Jaimes I, Le Borgne S (2003) Potential use of oxidative enzymes for the detoxification of organic pollutants. Appl Catal B: Environ 46: 1-15.
9. Gregory P (1986) Azo dyes: Structure-carcinogenicity relationships. Dyes Pigm 7: 45-56.
10. Cheon KS, Park YS, Kazmaier PM, Buncel E (2002) Studies of azo-hydrazone tautomerism and H-bonding in azo-functionalized dendrimers and model compounds. Dyes Pigm 53: 3-14.
11. Reeves RL, Kaiser RS (1970) Selective solvation of hydrophobic ions in structured solvents. Azo-hydrazone tautomerism of azo dyes in aqueous organic solvents. J Org Chem 35: 3670-3675.
12. Park H, Choi W (2003) Visible light and Fe(III)-mediated degradation of Acid Orange 7 in the absence of H_2O_2. J Photochem Photobiol A Chem 159: 241-247.
13. Zollinger H (1991) Color chemistry: syntheses, properties and application of organic dyes and pigments. 2nd edition. Weinheim: VCH.
14. Gregory P (2002) In: Hunger K (eds.). Industrial dyes: chemistry, properties and applications. Weinheim Wiley-VCH, pp: 543-585.
15. Clark RJH, Hester RE (1991) Advances in materials science spectroscopy. New York: John Wiley & Sons, USA.
16. Towns AD (1999) Developments in azo disperse dyes derived from heterocyclic diazo components. Dyes and Pigm 42: 3-28.
17. Marques MA, Gross EK (2004) Time-dependent density functional theory. Annu Rev Phys Chem 55: 427-455.
18. Wang Y, Wang J, Liu Y, Yang Y (2009) Theoretical Analysis of the Individual Contributions of Chiral Arrays to the Chiroptical Properties of Tris-diamine Ruthenium Chelates. J Am Chem Soc 131: 8839-8847.
19. Gao X, Wang Y, Jia J, Su X (2011) Sci Sin Chim 41: 1145-1155.
20. Frisch MJ, Pople JA (2004) Gaussian 03, Revision C.02, Gaussian Inc., Wallingford, CT.
21. Schlegel HB (1982) Optimization of equilibrium geometries and transition structures. J Comp Chem 3: 214-218.
22. Jamróz MH, Jan Cz D, Brzozowski R (2006) Vibrational modes of 2,6-, 2,7-, and 2,3-diisopropylnaphthalene. A DFT study. J Mol Struct 787: 172-183.
23. Michalska D, Program R (2003) The prediction of Raman spectra of platinum (II) anticancer drugs by density functional theory. Chemical Physics Letters 403: 211-217.
24. Glidewell C, Low JN, Skakle JMS, Wardell JL (2004) Hydrogen-bonded R22 (8) dimers in (E)-{[2-(phenyldiazenyl)phenyl]ethylideneaminooxy}acetic acid. Acta Cryst E60: o1560-o1562.
25. Biswns N, Umapathy S (1997) Density Functional Calculations of Structures, Vibrational Frequencies, and Normal Modes of trans- and cis-Azobenzene. J Phy Chem A 101: 5555.

26. Dos Santos HF, De Oliveira LFC, Dantas SO, Santos PS, De Almeida WB (2000) Quantum mechanical investigation of the tautomerism in the azo dye Sudan III. Int J Quan Chem 80: 1076-1086.

27. Bharanidharan S, Saleem H, Nathiya A, Arokiasamy A, Thanikachalam V (2015) Spectroscopic Investigations of (E)-5-(2-Phenyldiazenyl)-2-Hydroxybenzaldehyde Using DFT Method. Int Lett of Chem Phy and Astro 60: 168-181.

28. Scott AP, Radom L (1996) Harmonic Vibrational Frequencies: An Evaluation of Hartree−Fock, Møller−Plesset, Quadratic Configuration Interaction, Density Functional Theory, and Semiempirical Scale Factors. J Phys Chem 100: 16502-16513.

29. Michalska D, Bienko DC, Abkowicz-Bienko AJ, Latajka Z (1996) Density Functional, Hartree−Fock, and MP2 Studies on the Vibrational Spectrum of Phenol. J Phys Chem 100: 17786-17790.

30. Teimouri A, Chermahini AN, Taban K, Dabbagh HA (2009) Experimental and CIS, TD-DFT, ab initio calculations of visible spectra and the vibrational frequencies of sulfonyl azide-azoic dyes. Spectrochim Acta A 72: 369-377.

31. Varasanyi G (1974) Assignments for Vibrational Spectra of Seven Hundred Benzene Derivatives vol. 1-2 Adam Hilger.

32. Subramanian MK, Anbarasan PM, Manimegalai S (2009) Molecular structure, NMR and vibrational spectral analysis of 2,4-difluorophenol by ab initio HF and density functional theory. J Raman Spectrosc 40: 1657-1663.

33. Nuquist RA (1963) The O-H out-of-plane deformation in intramolecularly hydrogen bonded phenols. Spectrochim Acta 19: 1655-1664.

34. Snehalatha M, Ravikumar C, Hubert IJ (2009) Spectroscopic investigations and ab initio computations of the dye Chromotrope 2R. Solid State Sci 11: 1275.

35. Varsanyi G (1969) Vibrational Spectra of Benzene Derivatives, Academic Press, New York, USA.

36. Socrates G (1980) Infrared Characteristic group frequencies. John Wiley and Sons Ltd, New York, USA.

37. Bellamy LJ (1980) The infrared spectra of complex molecules. Chapman and Hall, London.

38. Vandenabeele P, Moens L, Edwards HGM, Dams R (2000) Raman spectroscopic database of azo pigments and application to modern art studies. J Raman Spectrosc 31: 509-517.

39. Trotter PJ (1977) Azo Dye Tautomeric Structures Determined by Laser-Raman Spectroscopy. Appl Spectrosc 31: 30-35.

40. Zyss J (1999) Molecular nonlinear optics: materials phenomena and devices. Chem Phys: 243.

41. Karna SP (2000) Electronics and optical materials: The Role of Theory and Modeling. J Phys Chem A 4671-4673.

42. Kanis DR, Ratner MA, Marks TJ (1994) Design and construction of molecular assemblies with large second-order optical nonlinearities. Quantum chemical aspects. Chem Rev 94: 195-242.

43. Xie S, Natansohn A, Rochon A (1993) Recent developments in aromatic azo polymers research. Chem Mater 5: 403-411.

44. Burland DM, Miller RD, Walsh CA (1994) Second-order nonlinearity in poled-polymer systems. Chem Rev 94: 31-75.

45. Liu ZF, Hashimoto K, Fujishima A (1990) Photoelectrochemical information storage using an azobenzene derivative. Nature 347: 658-660.

46. Ikeda T, Tsutsumi O (1995) Optical switching and image storage by means of azobenzene liquid-crystal films. Science 268: 1873-1875.

47. Kawata S, Kawata Y (2000) Three-Dimensional Optical Data Storage Using Photochromic Materials. Chem Rev 100: 1777-1788.

48. James C, Raj AA, Reghunathan R, Jayakumar VS, Hubert Joe I (2006) Structural conformation and vibrational spectroscopic studies of 2,6-bis(p-N,N-dimethyl benzylidene)cyclohexanone using density functional theory. J Raman Spectrosc 379: 1381-1392.

49. Liu J, Chen Z, Yuan S (2005) Study on the prediction of visible absorption maxima of azobenzene compounds. J Zhejiang Univ Sci 6B: 584-589.

50. Sebastian S, Sundaraganesan N (2010) The spectroscopic (FT-IR, FT-IR gas phase, FT-Raman and UV) and NBO analysis of 4-Hydroxypiperidine by density functional method. Spectrochim Acta A Mol Biomol Spectrosc 75: 941-952.

51. Luque FJ, Lopez JM, Orozco M (2000) Perspective on "Electrostatic interactions of a solute with a continuum. A direct utilization of ab initio molecular potentials for the prevision of solvent effects". Theor Chem Acc 103: 343-345.

52. Carthigayan K, Xavier S, Periandy S (2015) HOMO-LUMO, UV, NLO, NMR and vibrational analysis of 3-methyl-1-phenylpyrazole using FT-IR, FT-RAMAN FT-NMR spectra and HF-DFT computational methods. Spectrochim Acta A Mol Biomol Spectrosc 142: 350-363.